Controlling Battery Lifetime in a Battery Integrated Modular Multilevel Converter

1st Lars Leister
Elektrotechnisches Institut (ETI)
Karlsruhe Institute of Technology (KIT)
Karlsruhe, Germany
lars.leister@kit.edu

2nd Niklas Katzenburg
Elektrotechnisches Institut (ETI)
Karlsruhe Institute of Technology (KIT)
Karlsruhe, Germany
niklas.katzenburg@kit.edu

3rd Lukas Stefanski
Elektrotechnisches Institut (ETI)
Karlsruhe Institute of Technology (KIT)
Karlsruhe, Germany
lukas.stefanski@kit.edu

4th Marc Hiller
Elektrotechnisches Institut (ETI)
Karlsruhe Institute of Technology (KIT)
Karlsruhe, Germany
marc.hiller@kit.edu

***Abstract*—Due to the rising demand for energy storage systems within the electrical power grid, the modular multilevel converter with integrated batteries is discussed lately. With one advantage being the capability to incorporate second-life batteries, lifetime optimization is a key consideration to improve economic feasibility. In this paper, a new concept for battery lifetime optimization is established, implemented in the control structure and validated in a Hardware-in-the-Loop setup.**

***Index Terms*—Keywords—Modular Multi-level Converter, Energy Storage System, Battery Lifetime**

I. Introduction

The need for battery energy storage systems (BESS) in an electrical power grid with volatile sources and loads has been discussed extensively in society and science. While traditional BESS become increasingly common, more sophisticated approaches are still a niche topic. The capabilities of one such approach are discussed in this paper. The topology of a modular multilevel converter (MMC) [1] can be adapted to incorporate batteries within its submodules [2]–[5]. This approach brings the advantages of an MMC, such as high voltage quality and flexibility, to the realm of BESS. Due to the MMC's modular nature, different battery modules can be combined. This paper focuses on the combination of battery modules with identical voltage range but different capacity, current carrying capability and age. An approach to optimize the battery lifetimes while running the system under changing conditions is shown. Until now, the optimization objectives discussed in research range from state of charge (SoC)-Balancing [6] to multilayer equalization of the state of health (SoH) [7]. A brief overview of the literature is given in Tab. I.

Currently, optimizing the battery lifetime in such a system has rarely been discussed. SoH-balancing considers aging but does not necessarily increase battery lifetime. Rather, it results in all battery modules reaching theirEnd-of-Life (EOL) roughly simultaneously. However, this can become a disadvantage when aiming at operation without interruption. The exchange of a single battery module is possible during operation, while the exchange of all batteries at once disrupts operation. The influence of the current ripple from switching and harmonics of the grid current on the aging has also been discussed before, specifically for the MMC [8], [9]. According to this, reducing current harmonics can improve battery lifetime by decreasing losses, while switching frequencies do not have an evident effect on aging. It can also be argued that different operating scenarios require different balancing strategies [10]. However, this requires knowledge about the intended type of operation, which is not always given.

After an introduction to the MMC-BESS topology, this paper discusses a new concept to optimize battery lifetime. Each battery module is assigned two values: One will be called Need of Charge (NoC), indicating if charging the battery has a more positive or a more negative effect on the aging of that battery. The other will be called Need of Discharge (NoD), indicating the same for discharging. After those are established, balancing based on those values is applied in simulation of a simplified setup and in hardware-in-the-loop (HiL) emulation of the MMC-BESS. Finally, the paper gives an outlook on the feasibility for a real MMC-BESS.

TABLE I
Literature Overview of Balancing Methods for MMC-BESS

	Voltage	SoC	SoH	Lifetime
2011 - [11]	●	◐	○	○
2014 - [6]	●	●	○	○
2014 - [12]	●	●	○	○
2019 - [9]	◐	●	○	◐
2022 - [10]	○	●	●	○
2022 - [13]	○	●	○	○
2023 - [14]	●	●	○	○
2023 - [8]	○	○	○	◐

● = discussed ◐ = partly disc. ○ = not disc.

The project LeMoStore was funded by the Federal Ministry for Economic Affairs and Energy (BMWE) of Germany. The author is responsible for the content of this publication.

II. Topology

The MMC-BESS considered here [15] consists of multiple submodules called power electronic storage blocks (PESBs), each including a full bridge and a battery module. As shown in Fig. 1, the PESB^{z}_{xy} are arranged in three phases $y \in \{1,2,3\}$, each divided in a positive and negative arm $x \in \{\mathrm{p},\mathrm{n}\}$. The three phases are connected to the AC grid between their positive and negative arm. Per arm, $N = 20$ PESB indexed $z \in \{1,2...N\}$ and an arm inductor are connected in series.

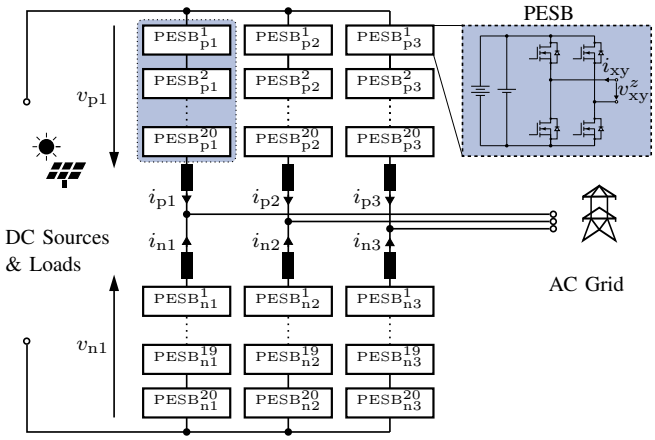

Fig. 1. Schematic of the MMC-BESS.

Energy distribution within the MMC-BESS has multiple aspects. On the battery cell level, balancing is crucial. Here, this is managed by the individual battery modules' battery management system (BMS) is not part of the MMC-control.

Energy distribution between submodules is the basis for the operation of a traditional MMC, where balancing the capacitor voltages is essential. The same control mechanisms can be employed to MMC-BESS to distribute energy. Balancing within one arm is done by prioritizing submodules in the selection process for voltage generation. The modulation of the arm voltages of the MMC is done using phase disposition pulse-width modulation (PWM). In short, the setpoint arm voltage is achieved by completely switching on a variable number of submodules, while one submodule sets a duty cycle $0 < d < 1$. For arm p1, this means that the battery of any $\mathrm{PESB}^{z}_{\mathrm{p1}}$ setting a positive output voltage v^{z}_{p1} while both the arm voltage v_{p1} and the arm current i_{p1} are positive, is charged. When i_{p1} is negative, the battery is discharged. Depending on AC and DC power, the polarity of i_{p1} can change at grid frequency. PESBs are typically sorted, so that modules with a higher priority for charging, i.e., due to lower voltage, are used more often and for longer durations during periods of positive current.

Additionally, balancing between arms is possible. Horizontal and vertical balancing can be differentiated; both require appropriate converter control and can result in additional internal currents and losses. While possible with the shown approach, they are not the focus of this work. Higher abstraction levels of energy distribution and optimization are also not discussed, e.g., the economic decision when to charge or discharge the BESS.

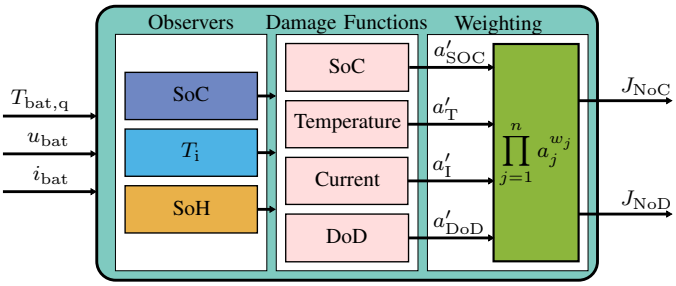

Fig. 2. Determination of Need of Charge and Need of Discharge.

III. Conceptualizing Need of Charge

To determine the charging and discharging priority of the battery modules, each battery is now assigned two values. They indicate whether charging and discharging have a more positive or negative effect on aging, respectively. In analogy to the term SoC, the term NoC is conceptualized here. The NoC is arbitrarily defined as a cost function J_{NoC} in the interval $[0,1]$. The lower this value, the faster the aging of the battery occurs when charging and vice versa. Analogously, the NoD is defined for discharging. Note that the SoH always decreases; the values of J_{NoC} and J_{NoD} simply imply whether it decreases faster or slower. A schematic to determine NoC and NoD is shown in Fig. 2 and is discussed in the following.

For both values, the current state of each battery must be determined first, which is done by observers for all quantities that cannot be measured directly. Given the battery status, damage functions are used to estimate the influence charging or discharging would have on the battery. Finally, these damage functions are normalized and a weighted product model is used to determine the NoC and the NoD.

A. Observers

Three observers are used to determine the SoC, the internal temperature of the battery cell T_{i} and the SoH in terms of the current battery capacity. To estimate the SoC, an Extended Kalman Filter (EKF) is implemented. It is parameterized based on [16] and uses lookup tables (LUTs) for the battery parameters. The measured battery module parameters are scaled to account for cells connected in parallel and series, as the modules used are configured as 14s22p. The additional connection resistance between the cells and within the module is assumed constant and proportionally added to the internal cell resistance.

The SoC-EKF is based on the Thevenin equivalent circuit model (ECM) shown in Fig. 3. For time step k, the input vector of the SoC-EKF is given depending on the battery cell current i_{cell} as

$$\underline{u}(k) = \begin{pmatrix} i_{\mathrm{cell}}(k-1) \\ \mathrm{sgn}(i_{\mathrm{cell}}(k-1)) \\ i_{\mathrm{cell}}(k) \end{pmatrix}. \tag{1}$$

The battery cell voltage is used as the measurement variable

$$z(k) = v_{\mathrm{cell}}(k). \tag{2}$$

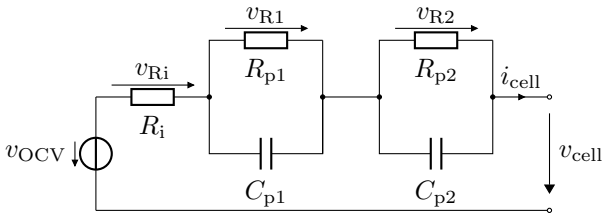

Fig. 3. Electrical Battery Cell Model.

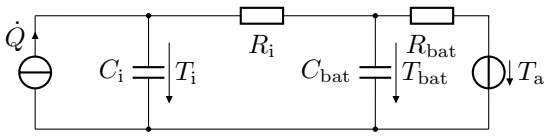

Fig. 4. Thermal Battery Cell Model.

The system state is denoted as

$$\underline{x}(k) = \begin{pmatrix} SoC(k) \\ v_{\mathrm{R1}}(k) \\ v_{\mathrm{R2}}(k) \\ v_{\mathrm{Ri}}(k) \end{pmatrix} \tag{3}$$

in accordance with the ECM. The open circuit voltage v_{ocv} and the SoC can be converted into each other by a LUT and are therefore interchangeable. The internal voltages $v_{\mathrm{Ri}}, v_{\mathrm{R1}}$ and v_{R2} calculated within the EKF represent the voltages over the internal resistance R_{i} and the RC networks used to approximate dynamic battery behavior, respectively.

To estimate the internal cell temperature T_{i}, a Kalman Filter (KF) similar to [17] is used. The thermal parameters are derived from measurements, a thermal ECM is shown in Fig. 4. The filter also increases the resolution of the estimated temperature T_{i} in comparison to the measured temperature $T_{\mathrm{bat,q}}$ from the BMS quantized with a resolution of 1 K. The system input is given by the ambient temperature T_{a} and the rate of heat flow $\dot{Q}$ resulting from the SoC-EKF as

$$\underline{u}(k) = \begin{pmatrix} \dot{Q}(k) \\ T_{\mathrm{a}}(k) \end{pmatrix}, \dot{Q}(k) = |i_{\mathrm{bat}} \cdot (v_{\mathrm{R1}}(k) + v_{\mathrm{R2}}(k) + v_{\mathrm{Ri}}(k))|. \tag{4}$$

The measurement variable is the quantized cell surface temperature $T_{\mathrm{bat,q}}$ coming from the BMS given as

$$z(k) = T_{\mathrm{bat,q}}(k) \tag{5}$$

while the system state $\underline{x}(k)$ is given as

$$\underline{x}(k) = \begin{pmatrix} T_{\mathrm{i}}(k) \\ T_{\mathrm{bat}}(k) \end{pmatrix}. \tag{6}$$

The latter consists of the internal battery cell temperature $T_{\mathrm{i}}(k)$ and the estimated battery surface temperature $T_{\mathrm{bat}}(k)$.

The SoH can be estimated by periodically cycling the battery modules. This has been shown for battery integrated MMCs, e.g., in [18] but is not discussed here. The SoH for simulation and HiL are given as model setpoints and not determined by an observer.

B. Damage Functions

Stress factors for battery aging are manifold [19]. Especially for second-life batteries, a precise lifetime estimation is hardly possible. Instead, a heuristic and real-time capable definition of the cost functions J_{NoC} and J_{NoD} for NoC and NoD is used, considering the following stress factors:

- **SoC** is a major driver for calendar aging. Based on [20], an exponential relation between SoC and aging is assumed where aging doubles at 100 % SoC and halves at 0 % SoC relative to the aging at 50 % SoC. This is expressed as

$$a_{\mathrm{SoC}} = 0.25 \cdot \mathrm{e}^{\ln 4 \cdot SoC} \tag{7}$$

and shown in Fig. 5. The higher this value is, the higher the NoD is supposed to be, while the NoC is supposed to decrease.

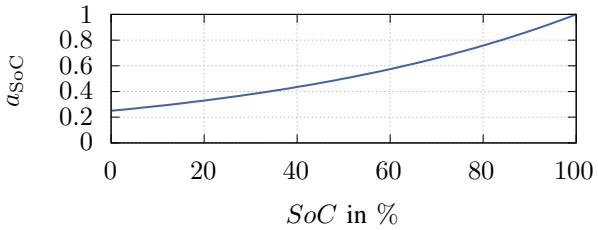

Fig. 5. Damage Function a_{SoC}.

- **Temperature** accelerates degradation processes for both calendar and cyclic aging for high and low temperatures. An average normal operation temperature range from −5 °C to 45 °C is chosen. To formulate the dependency, data for cyclic aging fitted to Arrhenius equations is used [21]. This yields

$$a_{\mathrm{T}} = \mathrm{e}^{b \cdot (T_{\mathrm{i}} - T_{\mathrm{ref}})} \text{ with } b = \begin{cases} 0.0232, & T_{\mathrm{i}} \geq T_{\mathrm{ref}} \\ -0.0579, & T_{\mathrm{i}} < T_{\mathrm{ref}} \end{cases} \tag{8}$$

and with $T_{\mathrm{ref}} = 25\,^{\circ}\mathrm{C}$ as shown in Fig. 6. The higher this value is, the lower both NoD and NoC are supposed to be.

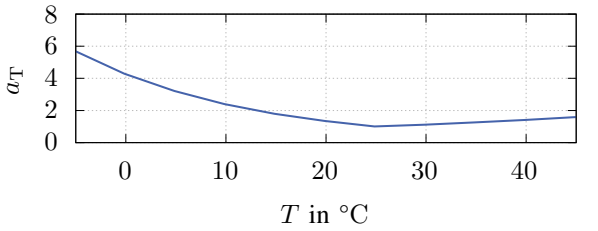

Fig. 6. Damage Function a_{T}.

- **Current/C-rate** leads to over- or undervoltage and any anode potential close to or below 0 V is known to accelerate Li-Plating. Depending on the temperature and the SoC, the current damage function is decribed as

$$a_{\mathrm{I}} = I_{\mathrm{max,C}}(SoC, T_{\mathrm{i}}) + I_{\mathrm{max,D}}(SoC, T_{\mathrm{i}}) \tag{9}$$

with the discharge current $I_{\mathrm{max,D}}$ being defined as negative. With this definition, higher values of a_{I} imply higher NoC and lower NoD. The data is derived from experimental cell data and given as LUTs. Exemplary data for $I_{\mathrm{max,C}}$ and $I_{\mathrm{max,D}}$ is shown in Fig. 7.

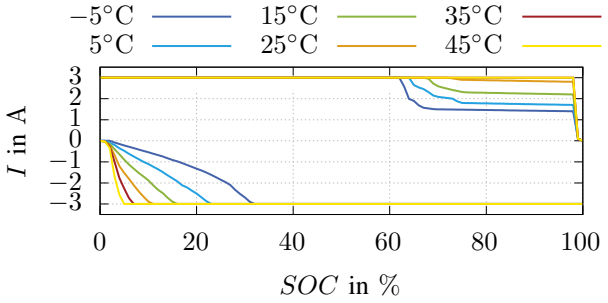

Fig. 7. Maximum Currents $I_{\mathrm{max,C}}$ and $I_{\mathrm{max,D}}$ as basis for a_{I}.

• **Depth of Discharge (DoD)** increases material fatigue. A real-time capable rainflow algorithm [5], [22] determines whether the current cycle belongs to a smaller subcycle or to a larger cycle. DoD,C and DoD,D are defined for charging and discharging, respectively. The Wöhler-Curve given as

$$a_{\mathrm{DoD,C/D}} = a \cdot DoD_{\mathrm{C/D}}^2 + b \cdot DoD_{\mathrm{C/D}} + c \quad \text{with } a = 1.4, b = 0.34, c = 0.032 \tag{10}$$

from [23] is adopted to quantify damage done to the battery by the DoD. The higher this value, the lower both NoC and NoD must become. Note that the DoD from a rainflow algorithm can be discontinuous over time. A smaller cycle becoming part of a larger cycle results in an abrupt increase in DoD.

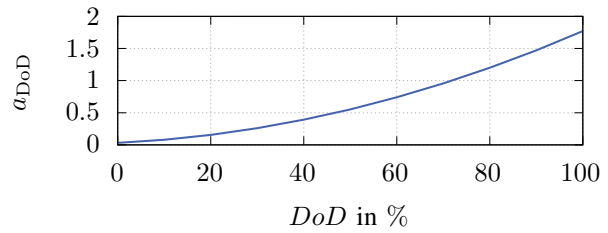

Fig. 8. Damage Function a_{DoD}.

Additionally, the actual current **Capacity** (SoH-dependent) is used to normalize NoC/NoD for different batteries and is denoted as a_{C}.

C. Weighting

All damage functions are rescaled to [0,1] with the rescaled damage functions being given as

$$a'_K = \frac{a_K - \min(a_K)}{\max(a_K) - \min(a_K)} \quad \text{with} K \in \{\mathrm{SoC,T,I,DoD_{C/D}}\}. \tag{11}$$

The minimum and maximum values are determined for the nominal range of operation. Furthermore, all stress factors are considered independent, i.e., do not influence each other. The cost functions J_{NoC} and the J_{NoD} are determined as the product of the rescaled damage factors. This weighted product model (WPM) is chosen to reflect the fact, that the damage functions cannot outweigh each other. For the NoC, the equation is given as

$$J_{\mathrm{NoC}} = (1 - a'_{\mathrm{SoC}})^{w_{\mathrm{soc}}} \cdot (1 - a'_{\mathrm{T}})^{w_{\mathrm{T}}} \cdot (a'_{\mathrm{I}})^{w_{\mathrm{I}}} \cdot (1 - a'_{\mathrm{DoD,C}})^{w_{\mathrm{DoD}}} \cdot (a_{\mathrm{C}})^{w_{\mathrm{C}}} \tag{12}$$

while for the NoD it is given as

$$J_{\mathrm{NoD}} = (a'_{\mathrm{SoC}})^{w_{\mathrm{soc}}} \cdot (1 - a'_{\mathrm{T}})^{w_{\mathrm{T}}} \cdot (1 - a'_{\mathrm{I}})^{w_{\mathrm{I}}} \cdot (1 - a'_{\mathrm{DoD,D}})^{w_{\mathrm{DoD}}} \cdot (a_{\mathrm{C}})^{w_{\mathrm{C}}}. \tag{13}$$

All damage functions are scaled to the expected range of operation so that all weighting factors w_K are set to 1 for the sake of simplicity. Different weights should be considered to change the relative relevance of specific factors. For example, increasing w_{SoC} might be considered for systems with long downtimes and thus increased calendar aging.

D. Implications

As an example for the implications of this approach, a battery resting at 25 °C and 50 % SoC is considered. Both charging and discharging reduce battery lifetime only as much as minimally possible due to the current throughput.+ For a battery at higher or lower temperature, aging increases so that both NoC and NoD decrease. Heating batteries at low temperatures by current throughput is not considered as lifetime improvement as the batteries in an MMC are thermally coupled and can therefore heat each other. For high SoC, NoC decreases while NoD increases. Ultimately, at $SoC = 100\,\%$, charging would result in overcharging, therefore $NoC = 0$ while $NoD = 1$ if all other stress factors were to be neglected. However, this approach is not intended to effectively prevent any kind of overload of the batteries. To prevent overcurrent even on short timescales, solutions limiting the current by limiting the duty cycle are superior [24]. To prevent operation outside the safe operating area, hard limits must be implemented in addition to NoC/NoD.

IV. Application in the MMC-BESS

To use the concept of NoC and NoD in the MMC, all 120 battery modules in the MMC-BESS must be monitored, the observers have to be executed, and J_{NoC} and J_{NoD} must be determined. Here, this is done by a real-time capable control platform [25] which also controls the converter itself. It is also used in the HiL setup introduced in [5], [26] and utilized here.

A. Hardware-in-the-Loop Evaluation

The NoC-balancing is implemented in a HiL-setup of the MMC-BESS as shown in Fig. 9. NoC and NoD are calculated on the ARM core of the Xilinx Z7030 system-on-chip. The control interrupt is executed at 8 kHz. The observers and the calculation of NoC and NoD are executed serially for each battery. Within one control clock period, the values for only one battery module are calculated to not exceed the interrupt duration. This is sufficient as the values are still updated at least once per grid period at 50 Hz. Sorting and modulation are running on the emulator FPGA. The MMC model on the emulator includes a state space converter model and ideal power electronic models for one arm. The electrical battery models are also running on the FPGA, while the thermal and aging models are running on the processor.

The applicability of the approach is shown in Fig. 10. The parameters of three exemplary battery modules are given in

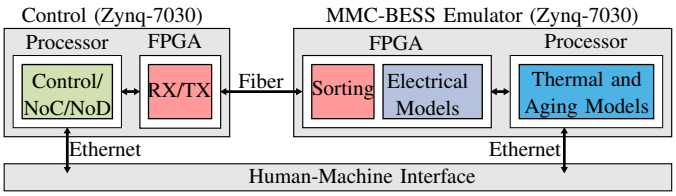

Fig. 9. Overview of the HiL Setup.

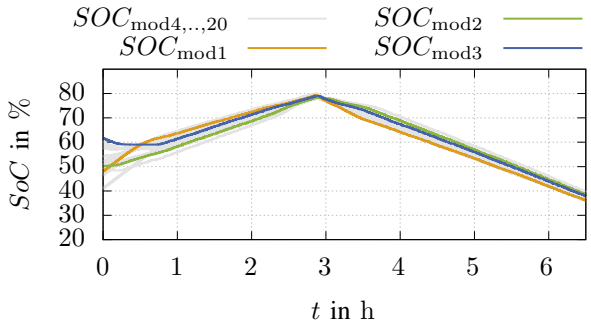

Fig. 10. Exemplary Power Profile and the SoC in HiL

Tab. II. For the first 3 h, the system reference power is in charging direction, after that it is discharging direction. As expected, Module 3 is not charged in the beginning due to its high SoC relative to the other modules. Module 2 is not charged as high as both module 1 and 3 at $t = 3\,\mathrm{h}$ due to its high SoH and low initial SoC. During charging, the behavior can be compared to SoC-balancing. This is expected as all modules are identical except for SoH. For some time during discharging, the SoCs somewhat diverge due to temperature and DoD differences but converge again when coming to lower SoC.

TABLE II
BATTERY PARAMETERS FOR HIL (EXTRACT) AND SIMULATION

Battery	SoC_{init}	SoH	T_{init} HiL	T_{init} Sim.
Module 1 (New)	47 %	97 %	25 °C	25 °C
Module 2 (Aged)	50 %	84 %	25 °C	45 °C
Module 3	60 %	88 %	25 °C	not applicable

B. *Simplified Simulation for Traceability*

The connections within the HiL model and the large number of modules make it difficult to verify the behavior. Therefore, Fig. 11 shows an exemplary behavior of NoC-balancing for two battery modules with mostly the same properties as the first two modules in HiL. The only difference is the higher temperature of Module 2 in simulation, as shown in Tab. II. An arbitrary total power reference over time is given and distributed between the two batteries according to the values calculated for J_{NoC} in Fig. 11 (i) and J_{NoD} in Fig. 11 (j). Fig. 11 (a) shows that both modules SoC's remain closely together although their capacity is different due to their respective SoH. The SoC of module 1 tends to reach lower and higher values than that of module 1. The main reason

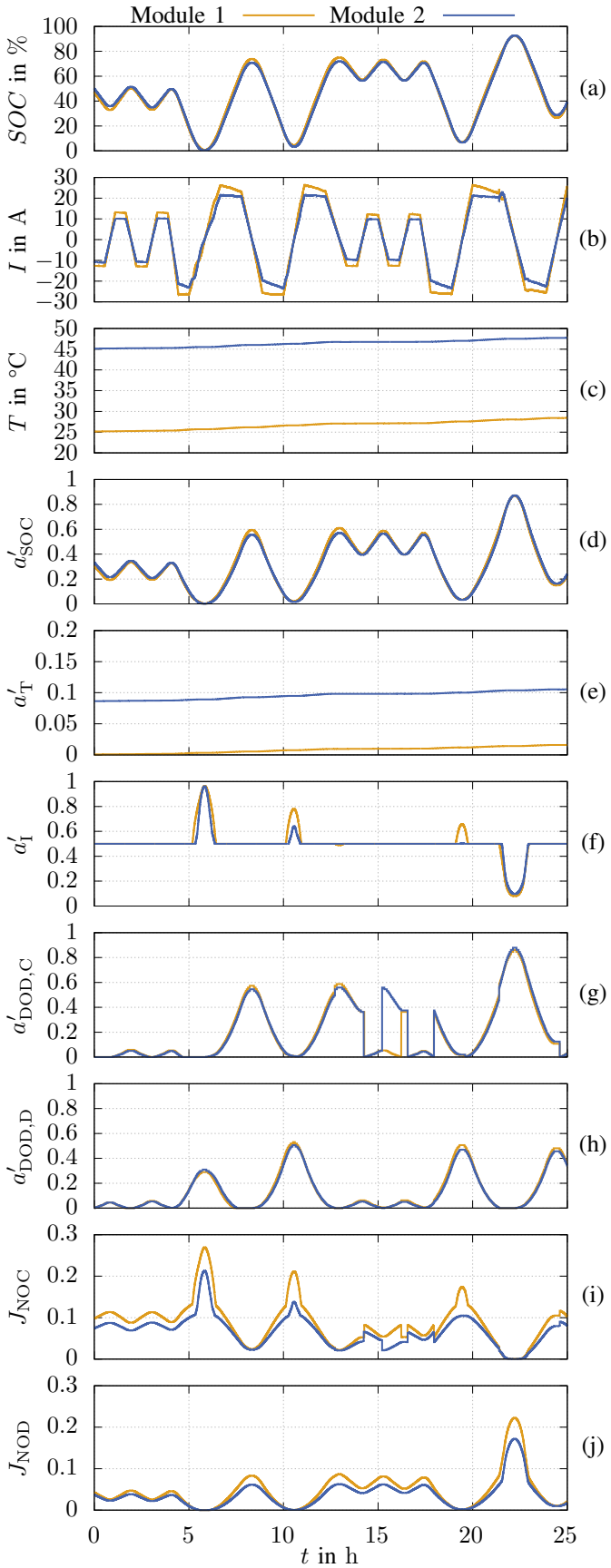

Fig. 11. Demonstration of the components of J_{NOC} and J_{NOD}

is given by the higher temperature of module 2 as shown in Fig. 11 (c) and the resulting damage function a'_{T} shown in Fig. 11 (e). As expected, the damage function a'_{soc} shown in Fig. 11 (d) follows the SoC and therefore supports the SoC-balancing. When high and low SoC are reached, a_{I} in Fig. 11 (f) comes into play. At around $5\,\mathrm{h}$ and $10\,\mathrm{h}$, the battery current distribution shifts back and forth between the two modules. The damage functions $a'_{\mathrm{DoD,C}}$ and $a'_{\mathrm{DoD,D}}$ are shown in Fig. 11 (g) and Fig. 11 (h) respectively. It is worth noting the behavior for module 2 at roughly $15\,\mathrm{h}$. $a'_{\mathrm{DoD,C}}$ jumps to the value from its previous half-cycle as soon as its SoC surpasses the maximum SoC of that previous cycle. After that, the value slowly decreases as the battery is discharged. When a new charging cycle starts at around $16\,\mathrm{h}$, $a'_{\mathrm{DoD,C}}$ starts from zero as a new half cycle begins. All in all, the behavior shows that all damage functions have the expected effect on the charging and discharging priority.

V. Conclusion and Outlook

The shown approach for power distribution within an MMC-BESS based on NoC and NoD allows lifetime optimized battery operation without prior knowledge of system operation mode. Combining the effect of multiple aging factors in the two variables NoC and NoD allows real-time application in the sorting algorithm of the MMC. This has been shown to work as intended in a HiL-environment while the individual impact of the included aging factors has been shown in a traceable simulation. The calculations have already been shown to be able to run on the real-time control system. Therefore, realization in a real MMC-BESS is straightforward and does not require changes. However, the quality of the observed variables in the real system must be determined and tested. In a next step, a comparison of the proposed method to established methods like SoC-balancing should be executed.

Acknowledgment

The authors acknowledge the battery cell data used in this paper provided by Batemo GmbH for the LeMoStore project.

References

[1] R. Marquardt, A. Lesnicar, and J. Hildinger, "Modulares Stromrichterkonzept für Netzkupplungsanwendungen bei hohen Spannungen," in *ETG-Fachtagung*, Bad Nauheim, Germany, 2002.

[2] M. Schroeder, S. Henninger, J. Jaeger, A. Raš, H. Rubenbauer, and H. Leu, "Integration of batteries into a modular multilevel converter," in *2013 15th European Conference on Power Electronics and Applications (EPE)*, Sep. 2013, pp. 1–12.

[3] A. Hillers, M. Stojadinovic, and J. Biela, "Systematic comparison of modular multilevel converter topologies for battery energy storage systems based on split batteries," in *EPE'15 ECCE-Europe*, Sep. 2015.

[4] M. Gommeringer, F. Kammerer, J. Kolb, and M. Braun, "Novel DC-AC Converter Topology for Multilevel Battery Energy Storage Systems," *PCIM Europe; proceedings*, p. 699, 2013.

[5] L. Leister, N. Katzenburg, K. Kuhlmann, L. Stefanski, and M. Hiller, "Faster than Real-Time Electro-Thermal-Aging Emulation of Multiple Batteries within a Modular Multilevel Converter," *EPE'23 ECCE Europe*, pp. 1–9, Aug. 2023.

[6] F. Gao, L. Zhang, Q. Zhou, M. Chen, T. Xu, and S. Hu, "State-of-charge balancing control strategy of battery energy storage system based on modular multilevel converter," in *2014 IEEE Energy Conversion Congress and Exposition (ECCE)*, Sep. 2014, pp. 2567–2574.

[7] Z. Ma, F. Gao, X. Gu, N. Li, Q. Wu, X. Wang, and X. Wang, "Multilayer SOH Equalization Scheme for MMC Battery Energy Storage System," *IEEE Transactions on Power Electronics*, vol. 35, no. 12, pp. 13 514–13 527, Dec. 2020.

[8] X. Straßer, G. W. Ngaleu, C. Hanzl, M. Azzam, C. Endisch, and M. Lewerenz, "Influence of Switching on the Aging of High Energy Lithium-Ion Cells," *Batteries*, vol. 9, no. 2, p. 139, Feb. 2023.

[9] D. Wang, J. Liu, L. Piegari, S. Song, X. Chen, and D. D. Simone, "A Battery Lifetime Improved Control Strategy of Modular Multilevel Converter for Electric Vehicle Application," in *2019 IEEE 10th International Symposium on Power Electronics for Distributed Generation Systems (PEDG)*, Jun. 2019, pp. 594–598.

[10] Z. Ma, F. Yu, X. Zhao, and F. Gao, "The Multidimensional Battery Management Strategy for MMC Battery Energy Storage System," in *7th Southern Power Electronics Conference (SPEC)*, Dec. 2022.

[11] I. Trintis, S. Munk-Nielsen, and R. Teodorescu, "A new modular multilevel converter with integrated energy storage," in *IECON 2011 - 37th Annual Conference of the IEEE IES*, Nov. 2011, pp. 1075–1080.

[12] F. Helling, S. Gotz, and T. Weyh, "A battery modular multilevel management system (BM3) for electric vehicles and stationary energy storage systems," in *2014 16th European Conference on Power Electronics and Applications*. Lappeenranta, Finland: IEEE, Aug. 2014, pp. 1–10.

[13] A. Alaa, A. Omar, A. Wood, H. Laird, and P. Gaynor, "Real-Time Emulation of a MMC with BESS for EV Application," Aug. 2022.

[14] A. Mashayekh, S. Pohlmann, J. Estaller, M. Kuder, A. Lesnicar, R. Eckerle, and T. Weyh, "Multi-Agent Reinforcement Learning-Based Decentralized Controller for Battery Modular Multilevel Inverter Systems," *Electricity*, vol. 4, no. 3, pp. 235–252, Sep. 2023.

[15] N. Katzenburg, K. Kuhlmann, L. Leister, L. Stefanski, J. Teigelkötter, and M. Hiller, "Design of a Modular Multilevel Converter with 400 kWh of Integrated Batteries," in *2023 22nd International Symposium on Power Electronics (Ee)*. Novi Sad, Serbia: IEEE, Oct. 2023.

[16] B. Rzepka, S. Bischof, and T. Blank, "Implementing an Extended Kalman Filter for SoC Estimation of a Li-Ion Battery with Hysteresis: A Step-by-Step Guide," *Energies*, vol. 14, no. 13, p. 3733, Jan. 2021.

[17] M. Liu, X. Zhou, L. Yang, and X. Ju, "A novel Kalman-filter-based battery internal temperature estimation method based on an enhanced electro-thermal coupling model," *Journal of Energy Storage*, vol. 71, p. 108241, Nov. 2023.

[18] Z. Ma, F. Gao, X. Gu, N. Li, and D. Niu, "An Online SOH Testing Method of MMC Battery Energy Storage System," in *19th Workshop on Control and Modeling for Power Electronics (COMPEL)*, Jun. 2018.

[19] S. S. Madani, Y. Shabeer, F. Allard, M. Fowler, C. Ziebert, Z. Wang, S. Panchal, H. Chaoui, S. Mekhilef, S. X. Dou, K. See, and K. Khalilpour, "A Comprehensive Review on Lithium-Ion Battery Lifetime Prediction and Aging Mechanism Analysis," *Batteries*, vol. 11, no. 4, p. 127, Apr. 2025.

[20] M. Uhrig, "Aspekte zur Integration stationärer und mobiler Batteriespeicher in die Verteilnetze," https://publikationen.bibliothek.kit.edu/1000072324, 2017.

[21] T. Waldmann, M. Wilka, M. Kasper, M. Fleischhammer, and M. Wohlfahrt-Mehrens, "Temperature dependent ageing mechanisms in Lithium-ion batteries – A Post-Mortem study," *Journal of Power Sources*, vol. 262, pp. 129–135, Sep. 2014.

[22] G. Marsh, C. Wignall, P. R. Thies, N. Barltrop, A. Incecik, V. Venugopal, and L. Johanning, "Review and application of Rainflow residue processing techniques for accurate fatigue damage estimation," *International Journal of Fatigue*, vol. 82, pp. 757–765, Jan. 2016.

[23] T. Grün, "Passiv gekoppelte Lithium-Ionen-Superkondensatorsysteme für 48V Hybridfahrzeuge," https://publikationen.bibliothek.kit.edu/1000127761, 2020.

[24] N. Katzenburg, L. Leister, L. Stefanski, and M. Hiller, "A Current-Based Submodule Selection Algorithm for a Modular Multilevel Converter with Integrated Batteries," in *10th IEEE Workshop on the Electronic Grid (eGrid 2025)*, Glasgow, Oct. 2025.

[25] B. Schmitz-Rode, L. Stefanski, R. Schwendemann, S. Decker, S. Mersche, P. Kiehnle, P. Himmelmann, A. Liske, and M. Hiller, "A modular signal processing platform for grid and motor control, HIL and PHIL applications," in *2022 International Conference on Power Electronics and ECCE Asia (IPEC-Himeji 2022 -ECCE Asia)*, 2022.

[26] L. Leister, A. Kalk, B. Schmitz-Rode, L. Stefanski, D. Bräckle, and M. Hiller, "Hardware-in-the-Loop Setup for a Modular Multilevel Converter with Integrated Batteries," in *2022 IEEE 23rd Workshop on Control and Modeling for Power Electronics (COMPEL)*, Jun. 2022.